JOC The Journal of Organic Chemistry

ARTICLE

pubs.acs.org/joc

Computational Mechanistic Study of PMe_3 and *N*-Heterocyclic Carbene Catalyzed Intramolecular Morita−Baylis−Hillman-Like Cycloalkylations: The Origins of the Different Reactivity

Lili Zhao,[†] Xiang Yu Chen,[‡] Song Ye,[‡] and Zhi-Xiang Wang*[,†]

[†]College of Chemistry and Chemical Engineering, Graduate University of Chinese Academy of Sciences, Beijing 100049, China

[‡]Beijing National Laboratory for Molecular Sciences, CAS Key Laboratory of Molecular Recognition and Function, Institute of Chemistry, Chinese Academy of Sciences, Beijing 100190, China

Supporting Information

ABSTRACT: It has been experimentally reported that PMe_3 catalyzes the cycloalkylation of the pendant halogenated α,β-unsaturated ketones (e.g., **1**) at the C^{α} position, whereas NHC catalyzes the cycloalkylation of the pendant halogenated α,β-unsaturated esters (e.g., **2**) at the C^{β} position. A DFT study has been performed to understand the detailed reaction mechanisms and the causes for the different ring closure positions in the two cycloalkylations promoted by the similar catalysts. Both reactions undergo three stages that include the nucleophilic addition of the catalysts (PMe_3 or NHC) to the substrates (**1** or **2**) and subsequent ring closure via S_N2 mechanism, the H-elimination by the bases (KOH or K_3PO_4), and the catalyst release giving the final products. The first stage in the NHC-catalyzed reaction involves a favorable H-transfer step leading to the umpolung Michael acceptor, which is more stable than the nucleophilic addition complex. The H-transfer turns off the possibility to close ring at C^{α} position for the reaction. In contrast, the similar H-transfer in the PMe_3-catalyzed reaction is thermodynamically unfavorable. According to the electronic structure of the addition complex of PMe_3 to substrate (**1**), we rationalize why the experimentally isolated intermediate in the PMe_3-catalyzed reaction is the *trans*-cyclic ketophosphonium salt, rather than its *cis* isomer that favors electrostatic attraction. The differences and the similarities among the two reactions and the traditional MBH reaction are discussed.

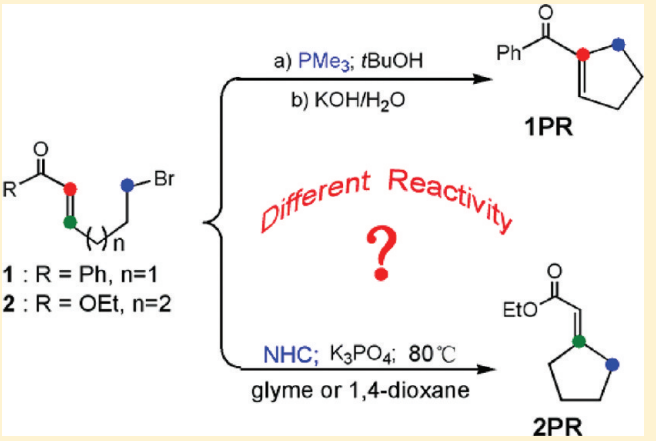

1. INTRODUCTION

The Morita−Baylis−Hillman (MBH) reaction[1,2] (e.g., eq 1), which couples α-carbon of activated alkenes with electrophiles under the influence of nucleophilic catalysts, provides a simple and convenient way to synthesize densely functionalized molecules.[3] While the electrophiles in the MBH reactions are often sp^2-hybridized carbon functional groups,[4] Krafft and co-workers[5] discovered that the electrophiles can be sp^3-hybridized carbon functional groups (e.g., the C−Br group in the pendant brominated α,β-unsaturated ketones (**1**)) in their intramolecular MBH-like reactions (e.g., eq 2). Similar to the MBH reactions, the C−C coupling in eq 2 takes place at the α-carbon position. Moreover, they successfully isolated an intermediate (the cyclic ketophosphonium salt),[6] which greatly contributes to understanding the mechanism of such reactions. Because the salt intermediate is not structurally preferable for the electrostatic attraction between the positive phosphorus and the negative carbonyl O centers,[7] they concluded that the role of the electrostatic attraction could be limited.[6]

In 2006, Fu and co-workers[8] had an unexpectedly discovery in their study intended to develop Ni- and Pd-catalyzed coupling of alkyl electrophiles. Interestingly, they found that,[8] under the catalysis of the *N*-heterocyclic carbene (NHC), the intramolecular C−C coupling in the pendant brominated α,β-unsaturated ester (**2**) takes place at the β-carbon (e.g., eq 3) rather than at α-carbon as in eq 2. The novel umpolung reactivity in eq 3 was expected to have the potential for the development of a new type of organocatalytic C−C coupling reactions.

To our knowledge, there has been no detailed mechanistic investigation on the two unprecedented reactions. We herein report a computational study to gain insight into the mechanisms of the two reactions, on the basis of which we discuss why similar substrates in the two reactions exhibit different reactivity.

Received: January 13, 2011
Published: March 04, 2011

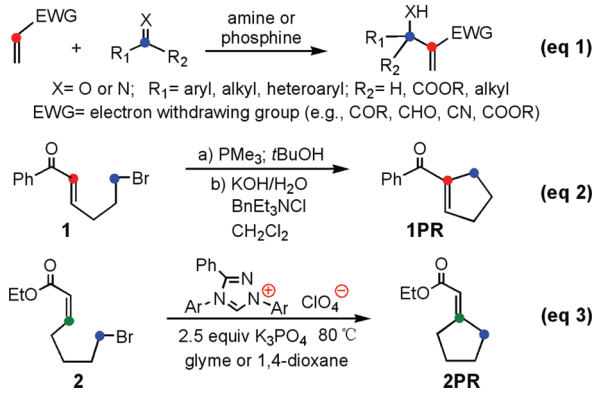

2. COMPUTATIONAL DETAILS

Our previous study[9] on the catalytic mechanism of NHC-catalyzed CO_2 transformation into methanol indicated that both geometric and energetic results from M05-2X DFT functional calculations account for the experimental observations well. The M05-2X functional,[10] as implemented in Gaussian 09 program,[11] was thus selected to carry out all DFT calculations. The realistic reaction system (including the catalysts and the substrates) were used without any simplification. All structures were optimized and characterized as minima or transition states at the M05-2X/6-31G* level. The energetic results were then improved by the single-point M05-2X/6-311++G**//M05-2X/6-31G* calculations with the solvation effects included. The bulky solvation effects, including the polarization effect and nonelectrostatic contribution, were simulated by the integral equation formalism polarizable continuum solvent model (IEFPCM).[12] Because the model for the experimentally used *t*BuOH solvent (eq 2) is not available in Gaussian, 2-BuOH was used for eq 2 reaction and 1, 4-dioxane for eq 3 reaction. (Note that the glyme solvent in eq 3 is also not available in Gaussian.) The gas phase M05-2X/6-31G* harmonic frequencies were used for thermal and entropic corrections to the enthalpies and free energies at 298.15 K and 1 atm. The natural bond orbital (NBO) analyses, performed by NBO 5.0[13] at the M05-2X/6-311++G** level, are applied to characterize the electronic structure of some species. The Gibbs free energies are used in the following discussion, unless otherwise specified, and the enthalpies are also given in the related schemes and figures.

3. RESULTS AND DISCUSSION

One of the goals of the study is to understand the causes for the different ring closure positions of the substrates **1** and **2** in the two reactions (eqs 2 and 3). We first investigate the detailed mechanism of the eq 2 (Section 3.1) and eq 3 (Section 3.2) reactions and then further discuss why the similar substrates exhibit the different reactivity in Section 3.3.

3.1. Mechanistic Details of the eq 2 Reaction (PMe_3-Catalyzed α-Cycloalkylation). For the eq 2 reaction, Krafft and co-workers isolated a cyclic ketophosphonium salt (**B** in Scheme 1) if the KOH base was not added.[6] On the basis of the structure of the salt, they have conceived that the reaction proceeds via the mechanism shown in Scheme 1.[6] To characterize the role of the base (i.e., KOH) and understand why the *trans*-cyclic ketophosphonium salt (**B**) could be isolated, we discuss the mechanism in terms of three stages: (I) formation of the cyclic ketophosphonium salt (**B**); (II) H^{α}-elimination promoted by KOH base; and (III) catalyst (PMe_3) release and the product (**1PR**) formation.

*Formation of the Cyclic Ketophosphonium Salt (**B/1-int3**): Stage I.* For the substrate, α,β-unsaturated ketone (**1**), the four major conformations shown in Supporting Information were considered and found to be close to each other with a free energy difference less than 2.0 kcal/mol. The most stable conformation (i.e., **1**) was used in our mechanistic study. The PMe_3 catalyst can possibly attack substrate **1** at the carbonyl carbon (C^{CO}), α-carbon (C^{α}), or β-carbon (C^{β}) positions, respectively. However, the complex of PMe_3 with **1** was highly unstable when attacking at the C^{CO} or could not be located when attacking at the C^{α} (see Supporting Information for details). This is in agreement with the general situation that nucleophilic catalysts prefer attacking activated alkenes at the C^{β} in the MBH reactions.[3,4] The first two scenarios can thus be ruled out, and we focus on the reaction via attacking at the C^{β} position. Figure 1 shows the energetic and geometric results for the favorable pathway.

Scheme 1. Schematic mechanism for the eq 2 reaction proposed by Krafft *et al.*

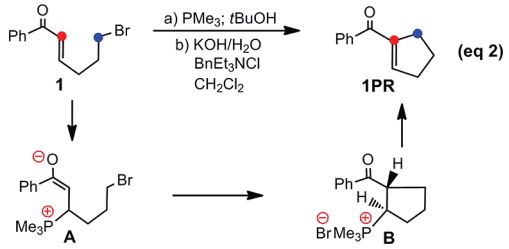

The attack of PMe_3 to the C^{β} of **1** initiates the reaction. Before forming the Lewis acid/base adduct (**1-int2**), the electrostatic attraction between the positive P-atom of PMe_3 and negative C^{β} center of **1** results in a complex (**1-int1**). The complex is enthalpically more stable but less stable in free energy than **1** + PMe_3, which implies that the electrostatic attraction can benefit the attack by pulling **1** and PMe_3 together. After crossing a barrier (**1-TS1**) of 19.3 kcal/mol, the Lewis acid/base adduct (**1-int2**) is formed. The addition process is illustrated by the gradually shortened $P-C^{\beta}$ distances, 3.536 Å in **1-int1**, 2.047 Å in **1-TS1** and 1.856 Å in **1-int2**. Manifested by the gradually elongated C^{α}-C^{β} bond distances, 1.336 Å in **1**, 1.431 Å in **1-TS1** and 1.479 Å in **1-int2**, the addition of PMe_3 to C^{β} weakens the C^{α}-C^{β} bonding. The Lewis acid/base complex (**1-int2**) is 11.7 kcal/mol higher than **1** + PMe_3. If there is no further driving force, the addition of PMe_3 to **1** could be difficult. However, the subsequent reaction step can provide driving force to move the reaction forward.

The addition of PMe_3 to **1** enhances the nucleophilicity of C^{α} center in **1-int2**, which facilitates the attack of the center to the electrophilic C^{ε} terminal via the S_N2 reaction mechanism. The reaction step closes the five-membered ring and makes Br^- leave simultaneously. Without PMe_3 catalysis, the intramolecular S_N2 reaction is unfavorable with a high barrier of 52.5 kcal/mol (see Supporting Information for detail). The PMe_3 catalyst facilitates the S_N2 reaction significantly; the barrier (**1-TS2**) is decreased to 22.8 kcal/mol. In **1-TS2**, the bond lengths of the forming $C^{\alpha}-C^{\varepsilon}$ and the breaking $C^{\varepsilon}-Br$ bonds are 2.215 and 2.407 Å, respectively, confirming the S_N2 transition state. The products of the S_N2 reaction (Br^--lost **1-int2** cation and Br^-) then combine to give the ion pair (**1-int3**). The stage I reaction giving **1-int3** is exergonic by 36.7 kcal/mol. **1-int3** corresponds to the isolated cyclic ketophosphonium salt (**B** in Scheme 1). The reasons for why **1-int3** can stably exist and thus can be isolated will be further discussed in combination with the energetic results of the stage II reaction.

dx.doi.org/10.1021/jo200087u |*J. Org. Chem.* 2011, 76, 2733–2743

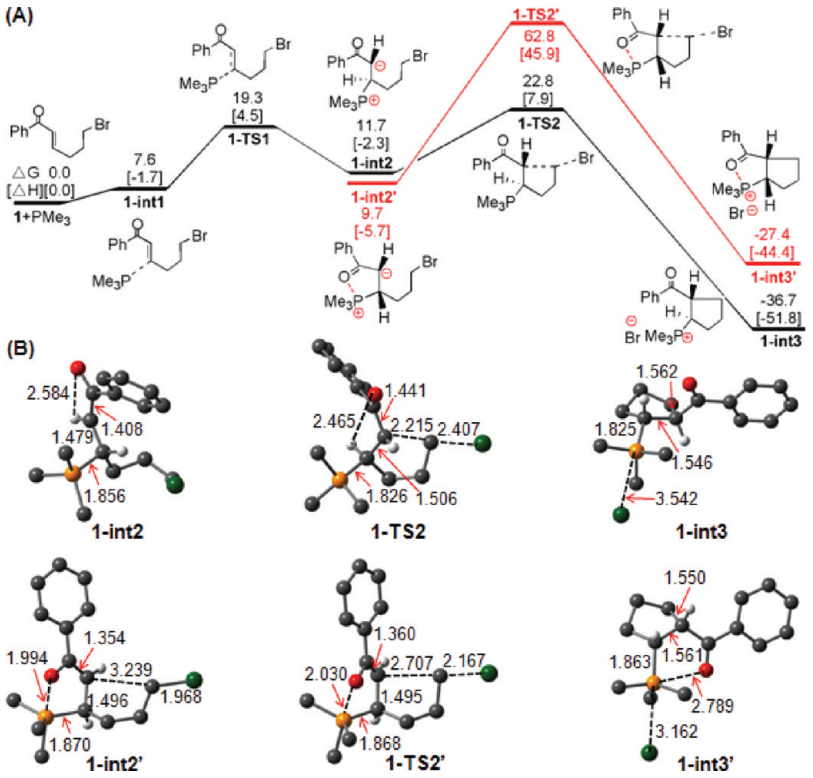

Figure 1. (A) Free energy profiles for the stage I of eq 2. Values in kcal/mol are free energies and enthalpies (in the brackets), respectively. (B) Optimized structures of key stationary points, along with the key bond distances in angstroms. Other optimized structures are given in Supporting Information. Trivial hydrogen atoms are omitted for clarity (color code, C: black, O: red, P: orange, Br: green, H: white).

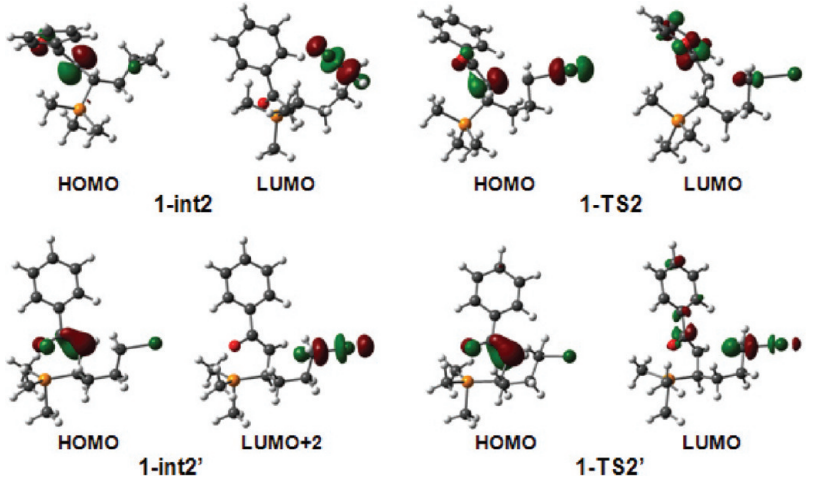

Figure 2. Comparisons of the molecular orbitals of **1-int2** and **1-TS2** related to the S_N2 reaction with those of **1-int2′** and **1-TS2′**.

The isolable intermediate (**1-int3**) is not structurally preferable for taking the advantage of the electrostatic attraction between the positive P- and negative O-centers.[7] Krafft et al. reasoned that the electrostatic attraction would not be important in this reaction.[6] To understand why the favorable electrostatic attraction cannot benefit the reaction, the intermediate (**1-int2′**) with structure in favor of the electrostatic attraction was also considered. Surprisingly, although **1-int2′** is even 2.0 kcal/mol lower than **1-int2**, the **1-TS2′** barrier (62.8 kcal/mol) is much higher than the 22.8 kcal/mol of **1-TS2**. We rationalize the significant barrier difference as follows.

To maximize the electrostatic attraction, as shown by the structure of **1-int2′** (Figure 1B), the H^{α} has to be *cis* to H^{β} in **1-int2′**, which is in contrast to the *trans* arrangement in **1-int2**. The different arrangements of the two H atoms lead to the different electronic structures. Figure 2 compares the molecular orbitals (MOs) of **1-int2** that are related to the S_N2 reaction with those of **1-int2′**. The HOMO of **1-int2** with an orbital energy (E_{oe} = −5.02 eV) is dominated by a lone pair located on the C^{α}, and the LUMO (E_{oe} = 1.05 eV) is the vacant C^{ε}−Br antibonding orbital to accept electrons from nucleophilic attacking group to break the bond. The ideal match of the two MOs and the small

dx.doi.org/10.1021/jo200087u |*J. Org. Chem.* 2011, 76, 2733–2743

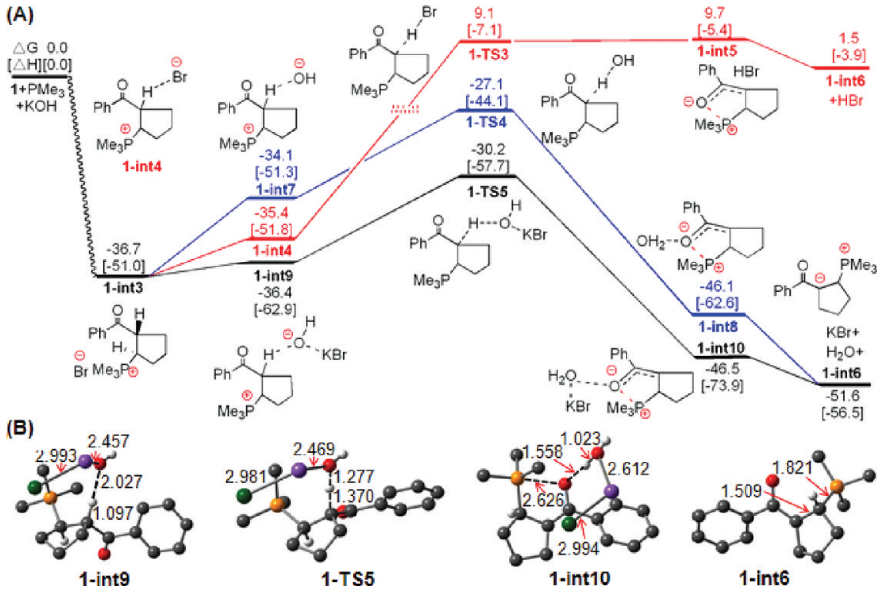

Figure 3. (A) Free energy profiles for stage II of eq 2. Values in kcal/mol are the free energies and enthalpies (in brackets), respectively. (B) Optimized structures of some important stationary points, along with the key bond distances in angstroms. Other optimized structures are given in Supporting Information. Trivial hydrogen atoms are omitted for clarity (color code, C: black, O: red, P: orange, Br: green, H: white, K: purple).

HOMO−LUMO gap (6.07 eV) suggest that the two MOs can interact effectively to undergo S_N2 reaction. In contrast, the HOMO of **1-int2′** is a partial π bonding orbital contributing to the $C^{CO}-C^{\alpha}$ bond. Because of the bonding character, the C^{α} of **1-int2′** is less nucleophilic than the C^{α} of **1-int2**, which is quantified by the lower E_{oe} (−6.46 eV) of HOMO in **1-int2′** compared with −5.02 eV in **1-int2**. Moreover, the empty C^{ε}-Br antibonding orbital of **1-int2′** is LUMO+2, instead of LUMO. The HOMO−(LUMO+2) gap (8.14 eV) is larger than the HOMO−LUMO gap (6.07 eV) of **1-int2**. The MO comparisons clearly indicate **1-int2** has more suitable electronic structure for the S_N2 reaction than **1-int2′**. In line with the different electronic structures, the $C^{CO}-C^{\alpha}$ bond length (1.408 Å) in **1-int2** is longer than the 1.354 Å in **1-int2′**. The HOMOs of **1-TS2** and **1-TS2′** also exhibit the similar differences (see Figure 2). The $C^{CO}-C^{\alpha}$ bond length (1.441 Å) in **1-TS2** is longer than the 1.360 Å in **1-TS2′**. Another contributor to the barrier difference is the steric effects. The *cis* arrangement of the H^{α} and H^{β} in **1-int2′** causes not only the different electronic structures but also relatively large steric repulsion, which along with the strain due to the five-membered $OC^{CO}C^{\alpha}C^{\beta}P$ ring destabilizes **1-int2′**. Because the favorable electrostatic attraction between P and O centers and the $C^{CO}-C^{\alpha}$ bonding interaction prevail over the destabilization factors, **1-int2′** is overall slightly more favorable than **1-int2**. As the S_N2 reaction proceeds, another five-membered ring begins to form. In **1-TS2′** two five-membered rings begin to fuse together, while there is only one five-membered ring in **1-TS2**. Obviously, the strain in **1-TS2′** is greater than that in **1-TS2**. Combing the electronic and steric effects together, it is not difficult to understand why **1-TS2′** is much higher than **1-TS2**. The steric effects are also responsible for why **1-int3′** is less stable than **1-int3**, but the energetic difference between **1-int3′** and **1-int3**, 9.3 kcal/mol, is much smaller than the 40.0 kcal/mol between **1-TS2′** and **1-TS2**, suggesting the different electronic structures is the major contributor to the much higher **1-TS2′** than **1-TS2**.

The generation of **1-int3** is kinetically and thermodynamically more favorable than the formation of **1-int3′**, although **1-int2** is slightly more unstable than **1-int2′**. This explains why the isolated intermediate is **1-int3**, rather than **1-int3′**. Following Krafft et al.'s proposal,[6] the other isomers of **1-int2** and **1-int2′** were also computed, but these isomers (see Supporting Information) are higher in energy than the two intermediates.

While the continuum solvent model was used to simulate the solvation effect,[12] the reaction system contains the polar molecules (i.e., *t*BuOH and H_2O, see eq 2). Can the explicit H-bond between the carbonyl group of **1** and *t*BuOH or H_2O molecules further facilitate this step? The corresponding pathways which explicitly include a *t*BuOH or H_2O molecule to form H-bond with the substrate **1** were investigated. The energetic and geometric results are detailed in Supporting Information. Comparing the energetic results of the two pathways with the reported values in Figure 1A, we observed that the presence of the direct H-bond can lower the barriers slightly in terms of enthalpy, but because of the enhanced entropic penalty due to the involvement of an additional molecule, the reaction pathways with explicit *t*BuOH or H_2O molecule becomes less favorable in terms of free energy. It can be concluded that the explicit H-bond between **1** and *t*BuOH or H_2O could not contribute to the reaction and the continuum solvent model should be adequate in the present study.

H^{α}-Elimination Promoted by Base (KOH): Stage II. After closing the five-memered ring in stage I, the reaction reaches the stage II to remove the protonic H^{α} atom (namely, H^{α}-elimination). To interpret the experimental fact that the salt (**1-int3**) can be isolated in the absence of strong base and that the strong base (i.e., KOH) was required to complete the whole reaction (eq 2),[6] the H^{α}-elimination pathways without or with KOH base were studied, and the energy profiles are presented in Figure 3, along with the optimized structures of some important stationary points.

In the absence of KOH base, the released Br^- from stage I can serve as the base to extract the H^{α} atom. The electrostatic

dx.doi.org/10.1021/jo200087u |*J. Org. Chem.* 2011, 76, 2733–2743

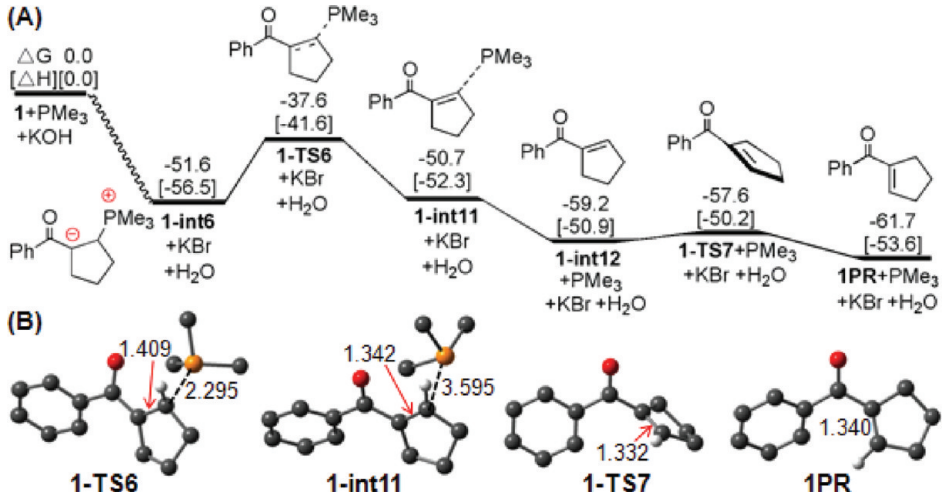

Figure 4. (A) Free energy profiles for the stage III of eq 2. Values in kcal/mol are free energies and enthalpies (in brackets), respectively. (B) Optimized structures of important stationary points, along with the key bond distances in angstroms. Trivial hydrogen atoms are omitted for clarity. (color code: C: black, O: red, P: orange, H: white).

Scheme 2. Complete Catalytic Cycle of the eq 2 Reaction

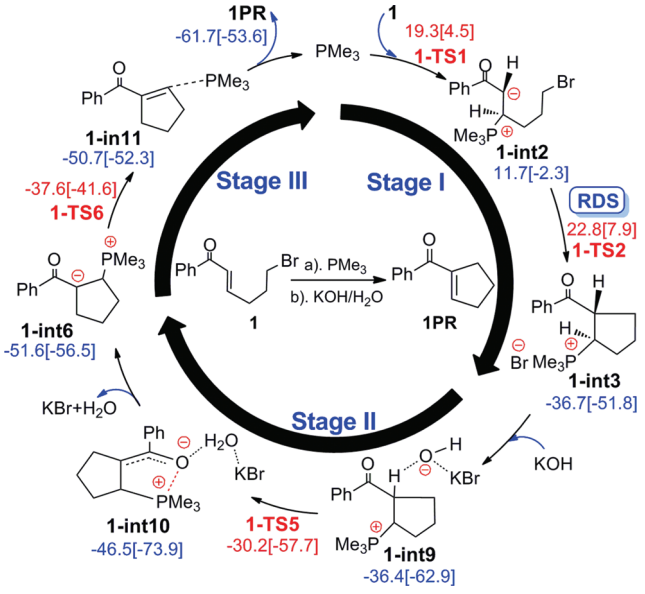

attraction between Br^- and the positive H^α first leads to the complex (**1-int4**) that is enthalpically more stable but less stable in free energy than **1-int3**. The barrier (**1-TS3**) for the H^α abstraction by Br^- is very high, 45.8 kcal/mol. The located H-bond complex (**1-int5**) is 13.0 kcal/mol more stable than **1-TS3** in the gas phase, however, it becomes slightly higher (0.6 kcal/mol) than **1-TS3** after solvation effects and thermal and entropic contributions accounted. Therefore, such a complex could not exist in the solution phase and does not affect the reaction. The products generated by the pathway, **1-int6** + HBr, are 38.2 kcal/mol higher than **1-int3**. The energy profile (the red path) indicates that **1-int3** is a deep minimum on the potential energy surface and thus is stable enough for its experimental isolation if no base is added. Note that, as discussed in stage I, the formation of **1-int3** is both kinetically and thermodynamically feasible (see Figure 1).

Scheme 3. Mechanism for NHC-Mediated β-Cycloalkylation of 2 Proposed by Fu et al.

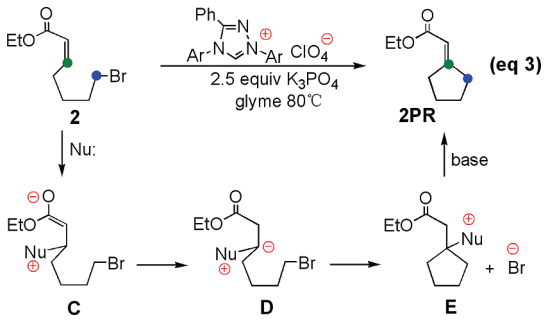

Br^- is not basic enough to achieve H^α-elimination and the reaction stops at **1-int3**. Experimentally, KOH base was used to drive the reaction forward.[6] In the presence of KOH base, two scenarios of H^α-elimination were considered. We first supposed that OH^- acts as a base to carry out the H^α-elimination alone (the blue path in Figure 3A). As expected, because of the stronger basicity of OH^- than Br^-, the H^α-elimination by OH^- becomes easier. The elimination barrier (**1-TS4**) by OH^-, 9.6 kcal/mol, is much lower than the 45.8 kcal/mol (**1-TS3**) by Br^-. Second, we assumed the released Br^- can form complex $BrKOH^-$ which then abstract H^α atom. As compared in Figure 3A, the $BrKOH^-$ complex can grab the H^α with even low free energy barrier; **1-TS5** is 3.1 kcal/mol lower than **1-TS4** in free energy. Therefore, the H^α-elimination can occur facilely in both scenarios. Comparison of the energy profile of H^α-elimination by Br^- and those either by OH^- and $BrKOH^-$ indicates a strong base (i.e., KOH) is required to move the reaction forward. The H^α-elimination products in the presence of KOH base, **1-int6** + H_2O + KBr are 51.6 kcal/mol more stable than **1** + PMe_3 + KOH.

All of the optimized structures of the stationary pointes labeled in Figure 3A are given in Supporting Information. As representatives, the optimized structures of **1-int9**, **1-TS5**, **1-int10** and **1-int6** along the most favorable H^α-elimination pathway are displayed in Figure 3B. The changes in the C^α—H^α

dx.doi.org/10.1021/jo200087u |J. Org. Chem. 2011, 76, 2733–2743

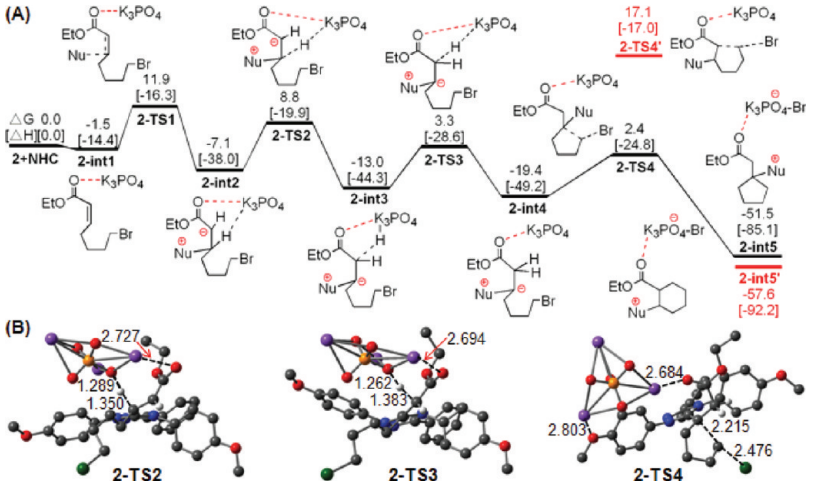

Figure 5. (A) Free energy profiles for the stage I of eq 3. Values in kcal/mol are free energies and enthalpies (in brackets), respectively. (B) Optimized structures of some important stationary points, along with the key bond distances in angstroms. Other optimized structures are given in Supporting Information. Trivial hydrogen atoms are omitted for clarity (color code: C: black, O: red, P: orange, Br: green, H: white, K: purple).

and $H^{\alpha}-O^{KBrOH}$ bond distances illustrate how the H^{α} elimination proceeds. It is worthy of noting that the two bond distances (1.370 and 1.227 Å, respectively) in **1-TS5** confirm the correct transition state.

We have reasoned above that, because the simultaneous presence of H^{α} and H^{β} results in larger steric effects in **1-int3′** than in **1-int3**, the former is less stable than the latter, although **1-int3′** has geometric structure in favor of the electrostatic attraction between the positive P- and negative O-centers (see Figure 1). In agreement with the reasoning, after losing the H^{α} atom via H^{α}-elimination, the intermediates (**1-int5**, **1-int8**, and **1-int10**) and the product (**1-int6**) of this stage all prefer structures in favor of electrostatic attraction.

*Catalyst (PMe_3) Release and the Product (**1PR**) Formation: Stage III.* In the second stage the H^{α}-elimination facilitated by KOH base changes **1-int3** into **1-int6**. In the stage III, the catalyst (PMe_3) is released from **1-int6**, leading to the final product (**1PR**). As indicated by the formal charges of **1-int6** (Figure 4), the formation of a $C^{\alpha}=C^{\beta}$ double bond push the catalyst PMe_3 away to produce the intermediate **1-int12**, in which the formed C=C bond and the carbonyl group are in the s-*cis* orientation. Subsequently, the formed five-membered ring can rotate along the $C^{CO}-C^{\alpha}$ single bond via a low barrier of 1.6 kcal/mol (**1-TS7**) leading to the more thermodynamically favorable product (**1PR**). The free energy barrier for releasing PMe_3 is 14.0 kcal/mol, and the product (**1PR** + PMe_3) is 10.1 kcal/mol lower than **1-int6**, indicating a kinetically and thermodynamically favorable process for liberating the catalysts.

Assembling the three stages together, the whole catalytic cycle of the eq 2 reaction is constructed in Scheme 2. Each of the three stages is kinetically feasible. The barrier (**1-TS2**) for the ring closure is the highest (22.8 kcal/mol) in the whole cycle, which indicates that the ring closure is the rate-determining step (RDS) in the whole cycle. The transition states (**1-TS2**, **1-TS5**, and **1-TS6**) are lower than the reactants (**1** + PMe_3 + KOH). As the reaction proceeds, the intermediate species become more and more thermodynamically stable, which provides force to drive the reaction forward to reach the final product (**1PR**).

3.2. Mechanistic Details of NHC-Mediated *β*-Cycloalkylation (eq 3). A striking difference between the eq 3 and eq 2 reactions is that the ring closure in eq 3 occurs at the C^{β} position,[8] rather than at the C^{α} position as in eq 2.[5,6] To reconcile the difference, Fu and co-workers[8] proposed a mechanism shown in Scheme 3. On the basis of their proposed mechanism and our understanding to the eq 2 reaction, we characterize the eq 3 reaction in terms of three stages similar to those of eq 2 reaction.

Scheme 4. Comparison of the Traditional Tautomerization with the H-Transfer

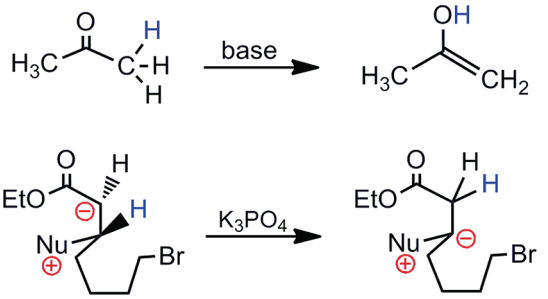

*Formation of the β-Cycloalkylated Zwitterionic Intermediate (**2-int5**): Stage I.* Similar to the consideration of substrate **1**, four conformations of the substrate **2** (α,β-unsaturated ester) were considered (see Supporting Information), and we used the most stable one in the mechanistic study. The energetic and geometric results for the stage I of the eq 3 reaction are shown in Figure 5. Different from the stage I in the eq 2 reaction, the stage I in the eq 3 reaction has an additional H transfer step from **2-int2** to **2-int4**.

For the eq 3 reaction, to generate NHC catalyst, the K_3PO_4 base presents at the beginning. We thus considered the reaction with K_3PO_4 involvement in the whole process. As shown in Figure 5A, a weak complex (**2-int1**) between K_3PO_4 and **2** could be located. The complex (**2-int1**) is −1.5 kcal/mol more stable than the separated **2** + K_3PO_4, which can be attributed to the weak electrostatic interactions between the K-atoms of K_3PO_4 and O^{CO}/Br atoms of **2**. The subsequent attack of NHC to **2** at the C^{β} position by passing a barrier of 13.4 kcal/mol (**2-TS1**)

dx.doi.org/10.1021/jo200087u |*J. Org. Chem.* 2011, 76, 2733–2743

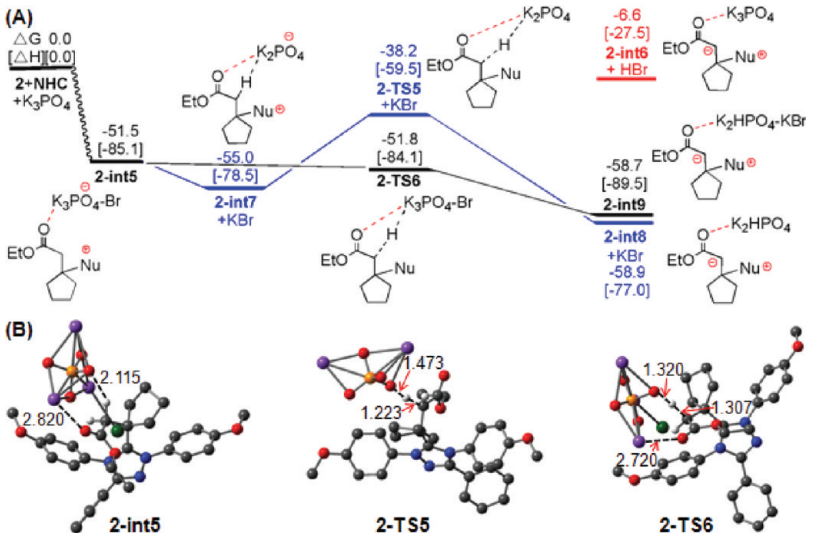

Figure 6. (A) Free energy profiles for the stage II of eq 3. Values are the free energies and enthalpies (in brackets) in kcal/mol, respectively. (B) Optimized structures of some important stationary points, along with the key bond distances in angstroms. Other optimized structures are given in Supporting Information. Trivial hydrogen atoms are omitted for clarity (color code, C: black, O: red, P: orange, Br: green, H: white, K: purple).

results in the zwitterionic **2-int2**. In comparison, for the direct addition of PMe_3 to **2** without the involvement of K_3PO_4 (details see Supporting Information), the corresponding barrier (**2-TS1′**) is 5.3 kcal/mol higher than **2-TS1** and the corresponding Lewis/acid adducts (**2-int2′**) is 13.3 kcal/mol less stable than **2-int2**. The comparisons indicate the participation of the K_3PO_4 base benefits the nucleophilic addition.

Subsequent to the formation of **2-int2**, the H atom on the C^{β} transfers to the C^{α}. Fu et al. proposed a tautomerization mechanism for the hydrogen transfer.[8] Inspired by their perspicacity, the H transfer mediated by K_3PO_4 base was first studied. Because the Br^- is not released until ring closure, we used K_3PO_4 as the sole promoter to examine how the H transfer is achieved. Based on our calculations, the H transfer takes place via the following mechanism. By overcoming a barrier (**2-TS2**), the H^{β} is first transferred to K_3PO_4 moiety, giving **2-int3** intermediate. The K_3PO_4−H moiety in **2-int3** then slightly adjusts its position to release the H atom to the C^{α} of the substrate by passing **2-TS3** transition state. The two barriers for the H abstraction and release are 15.9 and 16.3 kcal/mol, respectively. The process is also downhill: **2-int3** and **2-int5** are 5.9 and 12.3 kcal/mol more stable than **2-int2**. Therefore, the H transfer is kinetically and thermodynamically favorable, confirming Fu et al.'s proposal.[8] However, we call attention to the fact that the K_3PO_4-mediated H transfer is somewhat different from the classical base-catalyzed tautomerization. As compared in Scheme 4, the H migration in the tautomerization between enol and ketone takes place between carbonyl O atom and the C^{α}, whereas it happens between C^{α} and C^{β} in the K_3PO_4-mediated H transfer.

In addition to the K_3PO_4-mediated H transfer, we also explored other two mechanisms (see Supporting Information), including the direct intramolecular and intermolecular H transfers, without using base promoter. The barriers for the two H-transfer mechanisms, 39.3 and 32.5 kcal/mol, respectively, are much higher than that of **2-TS2** and **2-TS3**, which again demonstrate the important role of K_3PO_4 base except for generating the *in situ* NHC catalyst. Therefore, the K_3PO_4 base takes part in the reaction at the beginning of the reaction and accounts for why more base (2.5 equiv K_3PO_4) is required in eq 3.[8]

The H-transfer leads to the umpolung Michael acceptor **2-int4**. The nucleophilic C^{β} attack to the sp^3-hybridized alkyl bromine via a S_N2 reaction mechanism results in the closure of the five-membered ring at C^{β} position. The transition state **2-TS4** is 21.8 kcal/mol higher than **2-int4**. The ring closure product, **2-int5**, is thermodynamically favorable by −51.5 kcal/mol.

The study on the eq 2 reaction intrigued us to study if the ring closure in the stage I of eq 3 reaction can take place at the C^{α} position. Relative to the reactants, the energies of the barrier (**2-TS4′**) for the ring closure at C^{α} position and the ring closure product (**2-int5′**) were predicted to be 17.1 and −57.6 kcal/mol, respectively. The energies indicates that the ring closure at C^{α} position is also possible, but Fu et al. did not report the ring closure product (six-membered ring product).[8] In the following, we rationalize the experimental fact according to the energetic results. As shown in Figure 5, when the intermediate **2-int2** is formed after NHC addition, the reaction can proceed either by passing **2-TS2** to transfer H from C^{β} to C^{α} position or by overcoming **2-TS4′** to give **2-int5′**. Because K_3PO_4 facilitates transfer H from C^{β} to C^{α} position, the H transfer is thermodynamically favorable (downhill from **2-int2** to **2-int4**) and kinetically more favorable than the ring closure at C^{α} position (the two barriers for H transfer, **2-TS2** and **2-TS3**, are 8.3 and 13.8 kcal/mol lower than **2-TS4′**, respectively). Furthermore, the ring closure at C^{β} position via **2-TS4** is 14.7 kcal/mol more favorable than that at C^{α} via **2-TS4′**. In short, the ring closure is of kinetic control. In the case of eq 3 reaction, the more favorable kinetics of ring closure at C^{β} position than at C^{α} leads to the five-membered, rather than six-membered product. Note that, for a kinetically controlled reaction with two reaction channels, a free energy barrier difference of 5.0 kcal/mol can almost turn off the unfavorable reaction channel. For instance,[14] the enantiomeric excesses (ee) values could reach 99.99% if the barriers leading to the two enantiomers differ by 5.0 kcal/mol (details see Supporting Information). If no hydrogen transfer promoter is available, because, as predicted, the ring-closure at C^{α} is also energetically feasible, the ring closure would occur at C^{α} position, which is in agreement with the eq 2 reaction (see Figure 1). To verify this, it

dx.doi.org/10.1021/jo200087u |*J. Org. Chem.* 2011, 76, 2733–2743

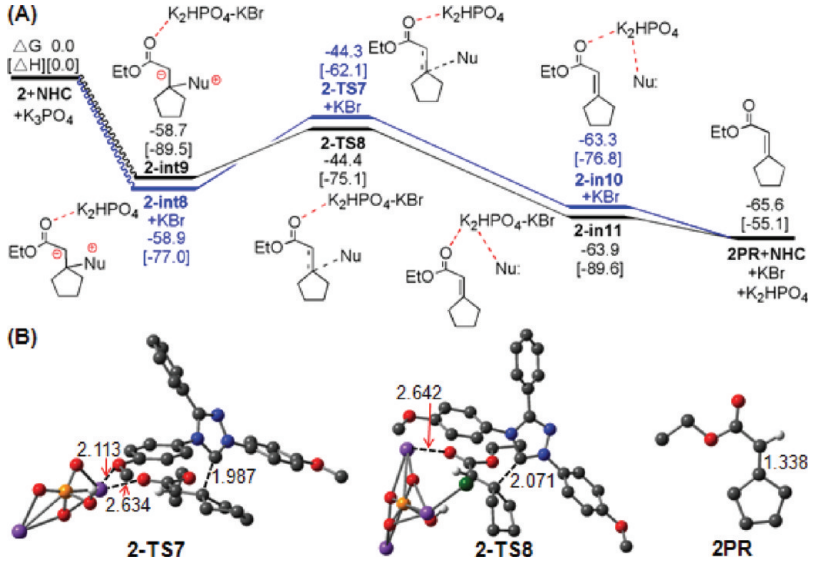

Figure 7. (A) Free energy profiles for the stage III of eq 3. Values in kcal/mol are free energies and enthalpies (in brackets), respectively. (B) Optimized structures of some important stationary points, along with the key bond distances in angstroms. Other optimized structures are given in Supporting Information. Trivial hydrogen atoms are omitted for clarity (color code, C: black, O: red, P: orange, Br: green, H: white, K: purple).

would be desirable to carry out an experimental study by using the same substrate but different catalysts.

H^{α}-Elimination: Stage II. After the ring closure to reach **2-int5**, H^{α}-elimination subsequently takes place in the stage II. Three scenarios of H^{α}-elimination were explored. In the first scenario, similar to the discussion in the stage II of eq 2, we considered the H^{α} abstraction by Br^{-} of K_3PO_4—Br moiety in **2-int5** to give **2-int6** + HBr (see Figure 6). Because the products (**2-int6** + HBr) are 44.9 kcal/mol higher than **2-int5**, this scenario is unfeasible. In the second scenario (blue path), because the reaction (**2-int5** → **2-int7** + KBr) is exothermic by 4.5 kcal/mol, we considered the H-abstraction by $K_2PO_4^{-}$ (the KBr is released). After crossing a barrier of 16.8 kcal/mol (**2-TS5**), the $K_2PO_4^{-}$ moiety in **2-int7** abstracts one of H^{α} atoms to generate the slightly more stable intermediate **2-int8**. The distances between the H^{α} and O of $K_2PO_4^{-}$ moiety (1.473 Å) and between the H^{α} and C^{α} (1.223 Å) confirm **2-TS5** to be the H abstraction transition state. In the third scenario (black path), the Br^{-} is also involved in the H^{α}-elimination pathway via the complex $BrK_3PO_4^{-}$. The transition state (**1-TS6**) is 13.6 kcal/mol lower than **1-TS5** and even 0.3 kcal/mol more stable than **2-int5** in free energy. Note that **2-TS6** is 4.9 kcal/mol higher than **2-int5** without any corrections. The H^{α}-elimination product, **2-int9**, is 58.7 kcal/mol more stable than **2** + NHC + K_3PO_4. We conclude both pathways are possible for the H^{α}-elimination.

*Catalyst (NHC) Release and the Product (**2PR**) Formation: Stage III.* The energetic and geometric results for the release of NHC starting from the complexes (**2-int8** or **2-int9**) to give finial product **2PR** are shown in Figure 7. To release NHC, the reaction needs overcome the barriers (**2-TS7** or **2-TS8**) that are 14.6 and 14.3 kcal/mol higher than **2-int8** or **2-int9**, respectively. The resultant complexes **2-int10** and **2-int11** are enthalpically favorable but less stable in free enthalpy than the final products **2PR** + NHC + KBr + K_2HPO_4. Thus the NHC catalyst can be easily liberated for the next cycle. Comparisons of the energetics in Figure 7 indicated that both pathways for catalyst

Scheme 5. Complete Catalytic Cycle of the eq 3 Reaction

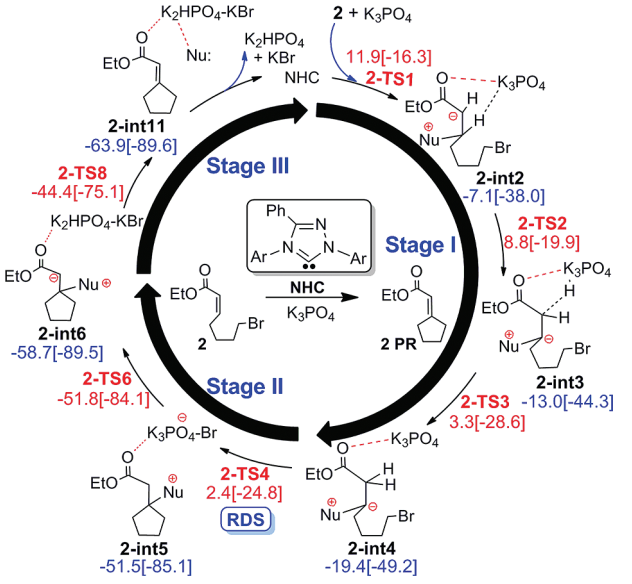

NHC release (starting from **2-int8** and **2-int9**, respectively) are kinetically and thermodynamically feasible.

On the basis of the detailed discussion on the eq 3 reaction, we assemble the three stages together to give the most favorable catalytic cycle in Scheme 5. As indicated by the energetic results, each stage is kinetically and thermodynamically feasible. As the reaction proceeds, the intermediate species become more and more thermodynamically favorable, which can afford driving force to reach the final product (**2PR**). The rate-determining step (RDS) for eq 3 reaction is predicted to be the C—C bond formation (ring closure) step, in which the barrier was predicated to be 21.8 kcal/mol.

3.3. Further Discussion. The mechanistic studies on the two reactions allow us to discuss why the similar substrates in the two

dx.doi.org/10.1021/jo200087u |*J. Org. Chem.* 2011, 76, 2733–2743

Table 1. Relative Free Energies and Enthalpies ($\Delta G[\Delta H]$, in kcal/mol) of int-B to int-A

Entry	Substrate	ΔG[ΔH] (PMe_3 catalyst)		ΔG[ΔH] (NHC catalyst)	
		2-BuOH[c]	1,4-dioxane[d]	2-BuOH	1,4-dioxane
1[a]	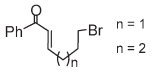 n = 1	12.4[10.3]	3.8[1.7]	-7.1[8.6]	-11.5[-13.0]
2[a]	n = 2	14.8[13.8]	7.6[6.6]	-6.0[-6.1]	-10.7[-10.8]
3[a]	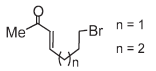 n = 1	17.5[14.9]	8.8[6.2]	-12.0[-9.7]]	-17.8[-15.5]
4[a]	n = 2	13.4[12.4]	5.4[4.5]	-10.3[-10.9]	-17.1[-17.7]
5[b]	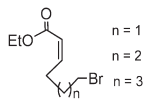 n = 1	14.9[12.5]	8.1[5.7]	-12.9[-11.9]	-17.3[-16.3]
6[b]	n = 2	12.3[10.6]	5.8[4.1]	-14.3[-12.3]	-18.2[-16.2]
7[b]	n = 3	14.8[13.8]	7.6[6.6]	-11.5[-8.0]	-13.4[-10.2]
8[b]	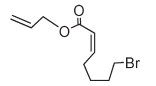	8.8[8.6]	3.1[2.9]	-12.0[-9.3]	-15.8[-13.1]

[a] Selected from Krafft et al.'s experiment. [b] Selected from Fu et al.'s experiment. [c] The solvent used in the calculation is 2-BuOH. [d] The solvent used in the calculation is 1,4-dioxane.

reactions exhibit different reactivity. According to the experiment by Fu et al.,[8] the H-transfer from C^{β} to C^{α} in eq 3 must occur, because the process switches off the possibility of ring closure at the C^{α} position and make the ring closure at the C^{β} position possibly to give the experimental product. Our calculations also show the H-transfer is indeed kinetically and thermodynamically feasible. This suggests that the isomerizatoin of **2-int2** into more stable **2-int4** via H-transfer could be a driving force to steer the ring closure at the C^{β} position. To examine the generality of the implication, we selected more substrates used in the Krafft et al.'s (entry 1−4)[5] and Fu et al.'s (entry 5−8)[8] experiments. The relative stability of the direct Lewis acid/base complexes (denoted as **int-A**) to their H-transfer isomers (**int-B**) is compared in Table 1.

From Table 1, it can be found that the substrates themselves have no essential influence on the relative stability of the two types of isomers. If NHC is used as catalyst, the **int-B** complexes are all more stable than the **int-A** complexes, regardless of the substrates used in either Krafft et al.'s[5] or Fu et al.'s[8] experiments. In contrast, the **int-B** complexes are all less stable than the **int-A** complexes if PMe_3 is utilized. Therefore, the difference between NHC and PMe_3 catalysts could be the determining factor for the different reactivity. Furthermore, the solvent effects of the two solvents favor the productions of the respective products. In the case of NHC catalyst, the 1,4-dioxane solvent stabilize **int-B**-type complexes more significantly than the 2-BuOH solvent to favor the ring closure at C^{β} position. In the case of PMe_3 catalyst, 2-BuOH solvent stabilize **int-A**-type complexes more significantly than 1,4-dioxane to favor the ring closure at C^{α} position.

Scheme 6 explains why PMe_3 and NHC lead to different relative stability of the two types of complexes. In the case of PMe_3, the zwitterionic **int-A**-type complex is more stable, because the P═C double bond (drawn in red) in **int-B** is less preferable. As for the case of NHC, the **int-B** complex can be well represented by the classical Lewis structure with C═C double bond, which results in the more stable **int-B**-type complexes. However, it should be pointed out that a driving force is required to achieve the H-transfer. As we discussed above, without additional mediator (i.e., K_3PO_4), both intramolecular and intermolecular

Scheme 6. Comparisons of the Two Types (int-A and int-B) of Complexes in the PMe_3- and NHC-Catalyzed Reactions

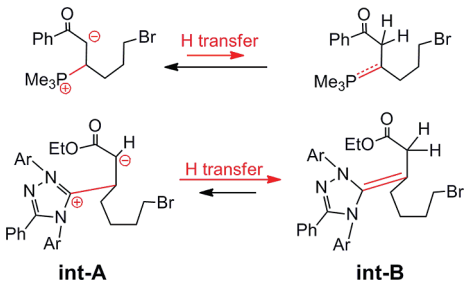

H transfer is not favorable (also see Suppporting Information). Therefore, a prompter such as K_3PO_4 used in eq 3 is required to promote the umpolung reactivity.[8]

Accordingly, we rationalize the ring closure at the C^{α} position in Krafft et al.'s experiments[5,6] (eq 2) from the following two aspects. On the one hand, the H transfer from C^{β} to C^{α} position is 12.4 kcal/mol thermodynamically unfavorable (see entry 1 in Table 1). On the other hand, there is no proper H-transfer mediator, because the KOH base is not presented at the beginning (i.e., stage I) of the reaction. Figure 8 illustrates the three H-transfer pathways in the eq 2 reaction. The intramolecular (the red path) and intermolecular (the green path) H-transfers are both highly unfavorable. The H-transfer via the *t*BuOH (the blue path) is also kinetically and thermodynamically unfavorable than the ring-closure pathway (the black path). Therefore, the hydrogen transfer from C^{β} to C^{α} in the eq 2 reaction is impossible, explaining why the α-cycloalkylated product **1PR** was obtained and accounts well for the kinetic experiment reported by Krafft and co-workers (no deuterium incorporation at the alkene *β*-position could be observed).[6]

Comparisons of the eq 2 and eq 3 reactions with typical MBH reaction (eq 1) show the following intriguing features: (i) The C−C coupling in the typical MBH reaction always takes place at the C^{α} position (eq 1),[3,4] which is similar to the ring closure at the C^{α} position in eq 2,[5,6] but is different from the ring closure at

dx.doi.org/10.1021/jo200087u |*J. Org. Chem.* 2011, 76, 2733–2743

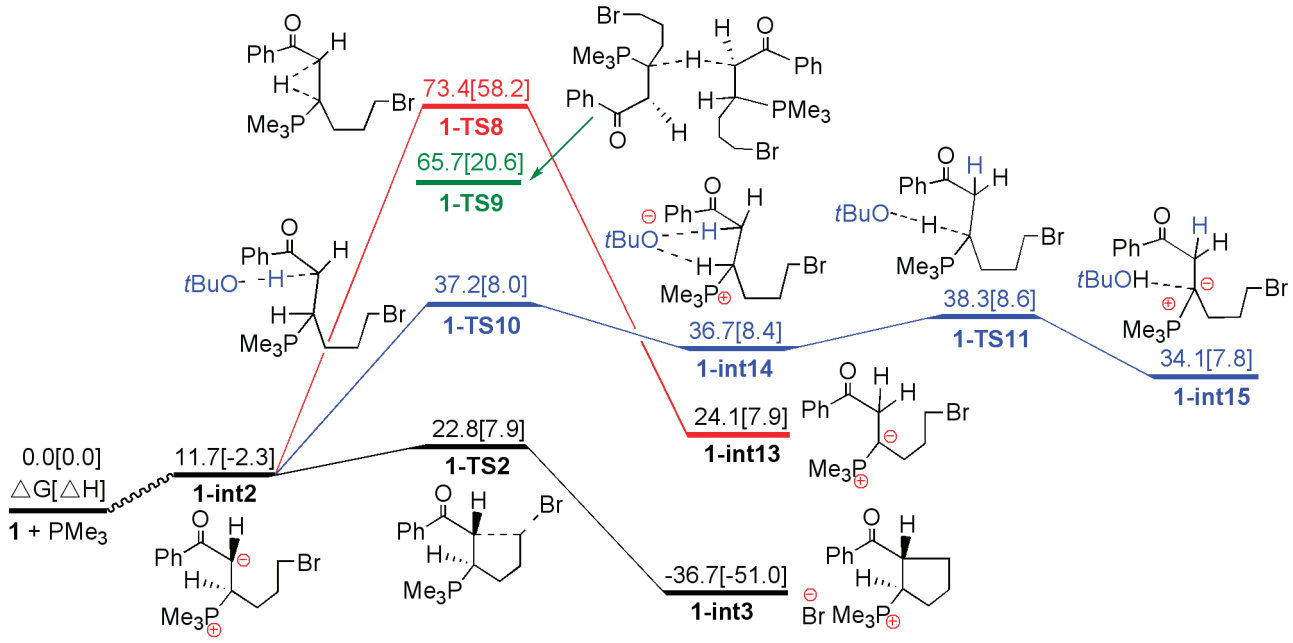

Figure 8. Free energy profiles for the H-transfer step of eq 2. Values in kcal/mol are free energies and enthalpies (in brackets), respectively. The optimized structures are given in Supporting Information.

the C^{β} position in eq 3.[8] (ii) Typical MBH reactions do not require base promoters, and all of the atoms in the reactants are transferred to the products. In contrast, the two reactions require base promoters. In the eq 2 reaction, the KOH base abstracts the protonic H^{α} to liberate the PMe_3 catalyst.[5,6] In the eq 3 reaction, the K_3PO_4 base not only creates NHC catalyst *in situ* but also mediates the H transfer and then abstract one protonic H^{α}.[8]

4. CONCLUSIONS

In conclusion, we have performed DFT calculations to study the detailed mechanisms of the PMe_3-mediated α-cycloalkylation reaction (eq 2) and the NHC-catalyzed *β*-cycloalkylation (eq 3). Both reactions takes place via three stages, including the attack of the nucleophilic catalyst (Lewis base) to the substrate at the C^{β} position and subsequent ring closure, the H-elimination promoted by the base, and the catalyst release by forming the C^{α}═C^{β} double bond. Our study accounts well for why the experimentally isolated intermediate in eq 2 is the *trans*-cyclic ketophosphonium salt, rather than the *cis* product. The study rationalizes why the ring closure take place at C^{α} position in eq 2 but at C^{β} in eq 3. The different reactivity in the two reactions originates from the different Lewis base catalysts. In the case of NHC, the H-transfer from C^{β} to C^{α} is thermodynamically favorable and a proper mediator is provided to promote the H-transfer. In the case of PMe_3, the H-transfer is intrinsically unfavorable. Thus even if there is a proper mediator, the H-transfer could be difficult to achieve. The eq 2 reaction is similar to the traditional MBH reactions in which the C−C coupling also takes place at the C^{α} position, but this is not the case in the eq 3 where the C−C coupling takes place at the C^{β} position. In principle, the two reactions are somewhat uivalent to the classical acid−base reaction.

■ ASSOCIATED CONTENT

Ⓢ Supporting Information. Geometric and energetic results for SI1, SI2, SI4−SI6, SI8, SI9, SI11, and SI12. Optimized structures of the stationary points that are schematically drawn in Figures 1A, 3A, 5A, 6A, and 7A but are not displayed in the main text. Cartesian coordinates, total enthalpies (**H**) and Gibbs free energies (**G**) of all stationary points involved in this study. This material is available free of charge via the Internet at http://pubs.acs.org.

■ AUTHOR INFORMATION

Corresponding Author

*E-mail: zxwang@gucas.ac.cn.

■ ACKNOWLEDGMENT

This work is supported by Chinese Academy of Sciences and the NFSC (Grant No. 20973197).

■ REFERENCES

(1) (a) Baylis, A. B.; Hillman, M. E. D.; German Patent 2155113, 1972; *Chem. Abstr.* **1972**, *77*, 34174q.

(2) (a) Morita, K. Japanese Patent 6803364, 1968; *Chem. Abstr.* **1968**, *69*, 58828s. (b) Morita, K.; Suzuki, Z.; Hirose, H. *Bull. Chem. Soc. Jpn.* **1968**, *41*, 2815.

(3) For reviews, see: (a) Basavaiah, D.; Rao, P. D.; Hyma, R. S. *Tetrahedron* **1996**, *52*, 8001. (b) Langer, P. *Angew. Chem., Int. Ed.* **2000**, *39*, 3049. (c) Basavaiah, D.; Rao, A. J.; Satyanarayana, T. *Chem. Rev.* **2003**, *103*, 811. (d) Carrasco-Sanchez, V.; Simirgiotis, M. J.; Santos, L. S. *Molecules* **2009**, *14*, 3989. (e) Basavaiah, D.; Reddy, B. S.; Badsara, S. S. *Chem. Rev.* **2010**, *110*, 5447.

(4) (a) Basavaiah, D.; Kumaragurubaran, N.; Sharada, D. S. *Tetrahedron Lett.* **2001**, *42*, 85. (b) Basavaiah, D.; Sharada, D. S.; Kumaragurubaran, N.; Reddy, R. M. *J. Org. Chem.* **2002**, *67*, 7135. (c) Jellerichs, B. G.; Kong, J. R.; Krische, M. J. *J. Am. Chem. Soc.* **2003**, *125*, 7758. (d) Koech, P. K.; Krische, M. J. *J. Am. Chem. Soc.* **2004**, *126*, 5350. (e) Luis, A. L.; Krische, M. J. *Synthesis* **2004**, 2579. (f) Krafft, M. E.; Haxell, T. F. N. *J. Am. Chem. Soc.* **2005**, *127*, 10168. (g) Xu, Y. M.; Shi, M. *J. Org. Chem.* **2004**, *69*, 417. (h) Shi, Y. L.; Shi, M. *Eur. J. org. Chem.* **2007**, 2905.

(i) Robiette, R.; Aggarwal, V. K.; Harvey, J. N. *J. Am. Chem. Soc.* **2007**, *129*, 15513. (j) Roy, D.; Sunoj, R. B. *Org. Lett.* **2007**, *9*, 4873. (k) Roy, D.; Sunoj, R. B. *Chem.—Eur. J.* **2008**, *14*, 10530. (l) Singh, V.; Batra, S. *Tetrahedron* **2008**, *64*, 4511. (m) Duarte, F. J. S.; Cabrita, E. J.; Frenking, G.; Santos, A. G. *Chem.—Eur. J.* **2009**, *15*, 1734. (n) Roy, D.; Patel, C.; Sunoj, R. B. *J. Org. Chem.* **2009**, *74*, 6936. (o) Cantillo, D.; Kappe, C. O. *J. Org. Chem.* **2010**, *75*, 8615.

(5) Krafft, M. E.; Seibert, K. A.; Haxell, T. F. N.; Hirosawa, C. *Chem. Commun.* **2005**, 5772.

(6) Krafft, M. E.; Haxell, T. F. N.; Seibert, K. A.; Abboud, K. A. *J. Am. Chem. Soc.* **2006**, *128*, 4174.

(7) Zhu, X. F.; Henry, C. E.; Kwon, O. *J. Am. Chem. Soc.* **2007**, *129*, 6722.

(8) Fischer, C.; Smith, S. W.; Powell, D. A.; Fu, G. C. *J. Am. Chem. Soc.* **2006**, *128*, 1472.

(9) Huang, F.; Lu, G.; Zhao, L. L.; Li, H. X.; Wang, Z. X. *J. Am. Chem. Soc.* **2010**, *132*, 12388.

(10) (a) Zhao, Y.; Schultz, N. E.; Truhlar, D. G. *J. Chem. Theory Comput.* **2006**, *2*, 364. (b) Zhao, Y.; Truhlar, D. G. *Acc. Chem. Res.* **2008**, *41*, 157.

(11) Frisch, M. J.; Trucks, G. W.; Schlegel, H. B.; Scuseria, G. E.; Robb, M. A.; Cheeseman, J. R.; Scalmani, G.; Barone, V.; Mennucci, B.; Petersson, G. A.; Nakatsuji, H.; Caricato, M.; Li, X.; Hratchian, H. P.; Izmaylov, A. F.; Bloino, J.; Zheng, G.; Sonnenberg, J. L.; Hada, M.; Ehara, M.; Toyota, K.; Fukuda, R.; Hasegawa, J.; Ishida, M.; Nakajima, T.; Honda, Y.; Kitao, O.; Nakai, H.; Vreven, T.; Montgomery, Jr., J. A.; Peralta, J. E.; Ogliaro, F.; Bearpark, M.; Heyd, J. J.; Brothers, E.; Kudin, K. N.; Staroverov, V. N.; Kobayashi, R.; Normand, J.; Raghavachari, K.; Rendell, A.; Burant, J. C.; Iyengar, S. S.; Tomasi, J.; Cossi, M.; Rega, N.; Millam, N. J.; Klene, M.; Knox, J. E.; Cross, J. B.; Bakken, V.; Adamo, C.; Jaramillo, J.; Gomperts, R.; Stratmann, R. E.; Yazyev, O.; Austin, A. J.; Cammi, R.; Pomelli, C.; Ochterski, J. W.; Martin, R. L.; Morokuma, K.; Zakrzewski, V. G.; Voth, G. A.; Salvador, P.; Dannenberg, J. J.; Dapprich, S.; Daniels, A. D.; Farkas, Ö.; Foresman, J. B.; Ortiz, J. V.; Cioslowski, J.; Fox, D. J. *Gaussian 09, Revision A.1*; Gaussian, Inc.: Wallingford, CT, 2009.

(12) (a) Mennucci, B.; Tomasi, J. *J. Chem. Phys.* **1997**, *107*, 3032. (b) Mennucci, B.; Tomasi, J. *J. Chem. Phys.* **1997**, *107*, 5151. (c) Mennucci, B.; Cancès, E.; Tomasi, J. *J. Phys. Chem. B* **1997**, *101*, 10506. (d) Tomasi, J.; Mennuncci, B.; Cancès, E. *J. Mol. Struct.* **1999**, *464*, 211.

(13) Glendening, E. D.; Badenhoop, J. K.; Reed, A. E.; Carpenter, J. E.; Bohmann, J. A.; Morales, C. M.; Weinhold, F. *NBO. 5.0*; Theoretical Chemistry Institute, University of Wisconsin: Madison, WI, 2001.

(14) Schneebeli, S. T.; Hall, M. L.; Breslow, R.; Friesner, R. *J. Am. Chem. Soc.* **2009**, *131*, 3965.